

# Thermal Analysis of Amorphous Phases in Hydroxyapatite Coatings

Karlis A. Gross,<sup>†,‡</sup> Volfgangs Gross,<sup>§</sup> and Christopher C. Berndt<sup>\*,†</sup>

Thermal Spray Laboratory, Department of Materials Science and Engineering, State University of New York at Stony Brook, Stony Brook, New York 11794-2275

Division of Materials Science and Technology, Commonwealth Scientific Industrial Research Organization, Clayton, 3168, Australia

**The amorphous phase in hydroxyapatite coatings has been examined by using X-ray diffractometry, Fourier transform infrared spectroscopy, optical microscopy, and thermal analysis methods. The amorphous phase mostly consists of a dehydroxylated calcium phosphate. When heated, crystallization of hydroxyl-rich areas produces hydroxyapatite, followed by diffusion of hydroxyl ions, thus increasing the amount of crystalline phase. Hydroxyl-deficient amorphous areas crystallize to oxyapatite at 700°C. Thus, crystallization occurs over a range of temperatures and is dependent on the hydroxyl content of the amorphous phase and the partial water-vapor pressure. The activation energies of crystallization to hydroxyapatite, diffusion of hydroxyl ions, and crystallization to oxyapatite are 274, 230, and 440 kJ/mol, respectively. Shrinkage from these processes leads to a crack network and decreases the mechanical strength of the coating.**

## I. Introduction

**H**YDROXYAPATITE is used as a coating on orthopedic and dental implants to enhance fixation of the implant to the surrounding bone.<sup>1,2</sup> Hydroxyapatite coatings that are prepared via plasma spraying typically consist of a mixture of crystalline and amorphous phases.<sup>3</sup> The amorphous phase, when located on the outer surface of a coating, promotes the growth of osseous tissue, compared to crystalline sintered hydroxyapatite.<sup>4</sup> However, the high dissolution of the amorphous phase<sup>5</sup> could influence implant stability. The location of the amorphous phase can especially be detrimental, in the long term, if the amorphous phase is located in regions that are adjacent to the substrate, where preferential dissolution of the amorphous phase can lead to delamination and, hence, implant failure.

One way of controlling the amount of amorphous phase is by heat treatment after the spraying procedure.<sup>6</sup> The formation of crystalline hydroxyapatite at the coating/substrate interface via heat treatment has several advantages. Crystallization of any amorphous phase that is adjacent to the substrate will lower the dissolution and improve the substrate-coating bond strength.<sup>7</sup> The cohesive properties of the coating will also be improved.

Post-heat-treatment has been used to study the crystallization of the amorphous phase in ion-beam-deposited amorphous coatings, and the process has been investigated by using electron microscopy.<sup>8</sup> Some studies have begun to address crystallization in plasma-sprayed coatings using X-ray diffractometry (XRD).<sup>9,10</sup> This work uses Fourier transform infrared (FTIR)

spectroscopy, XRD, microscopy, and thermal analysis methods (differential thermal analysis (DTA), thermal gravimetric analysis (TGA), and dilatometry) to examine the chemical and physical changes that occur in the coating as a result of heat treatment of the amorphous phase. The knowledge of the physiochemical changes that is gained from this study may then also be extended to control crystallization that may occur during the processing stage.

## II. Methods

### (1) Amorphous-Phase Production

Atmospheric plasma spraying (with a Metco 3MB gun (Sulzer Metco, Westbury, NY) and a GH nozzle) offers very fast cooling rates ( $\sim 10^6$ °C/s) and was used to produce amorphous coatings. Argon was selected as the primary gas, and nitrogen was added to increase the enthalpy of the plasma and adjust the power level to 25 kW. A stand-off distance of 15 cm ensured an acceptable deposition efficiency. Spherical hydroxyapatite powder with a Ca:P ratio of 1.67 and a particle-size distribution of  $<40 \mu\text{m}$  (Fig. 1) was injected externally to the gun, perpendicular to the plasma plume. A coating was formed on a lightly grit-blasted titanium substrate (roughness,  $R_a$ , of 3  $\mu\text{m}$ , compared to the usual value of 7  $\mu\text{m}$ ) to encourage better spreading of the molten particles; this produces higher cooling rates and facilitates the ease of coating removal from the substrate. Air cooling and a high torch traverse speed were both chosen to avoid heating the substrate. The coatings were removed from the substrate immediately after manufacture and placed in a desiccator.

### (2) Chemical and Phase Analysis

The starting powder and the amorphous phase were examined for calcium and phosphorus content; a Ca:P molar ratio of 1.67 represents stoichiometric hydroxyapatite. Calcium was determined with atomic mass spectroscopy, and phosphorus was measured by using an inductively coupled plasma (ICP) technique.

XRD analysis was performed using  $\text{CuK}\alpha_1$  radiation with a wavelength,  $\lambda$ , of 1.54 Å (0.154 nm); the operating conditions were 40 kV and 30 mA. The goniometer was set at a scan rate of 0.01° 2 $\theta$ /s over a 2 $\theta$  range of 20°–60°.

### (3) Thermal Gravimetric Analysis/Differential Thermal Analysis

The amorphous coating was ground in a mortar and pestle and placed in an alumina ( $\text{Al}_2\text{O}_3$ ) crucible for analysis. The crucible was heated at a rate of 5°C/min to a temperature of 1400°C in either air or helium, and the weight was continually monitored. The error in weight measurement was  $-0.25 \text{ wt}\%$ .

DTA was performed along with TGA, which enabled changes in weight to be correlated with reactions that were observed in the DTA trace. The error in the signal was  $-5.7 \mu\text{V/g}$ .

The peak temperature of an exothermic or endothermic reaction occurs at higher temperatures as the heating rate is increased; this is linked to the reaction kinetics and can be used

P. W. Brown—contributing editor

Manuscript No. 191386. Received November 11, 1996; approved May 6, 1997.

<sup>†</sup>Member, American Ceramic Society.

Thermal Spray Laboratory, SUNY.

<sup>\*</sup>Author to whom correspondence should be addressed. Presently at Dept. of Materials Engineering, Monash University, Clayton 3168, Australia.

<sup>§</sup>Division of Materials Science and Technology, CSIRO.

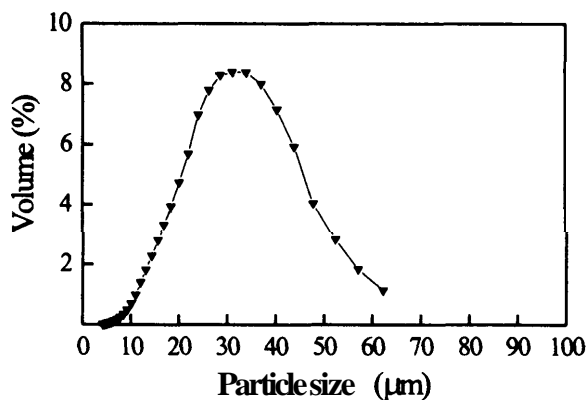


Fig. 1. Particle-size distribution of hydroxyapatite powder used in plasma spraying.

to calculate the activation energy of a process. Kissinger<sup>11</sup> developed a method whereby the activation energy of crystallization<sup>12,13</sup> can be calculated from plotting  $\ln(\Phi/T_p^2)$  against  $T_p^{-1}$  ( $\Phi$  is the heating rate and  $T_p$  is the temperature of the peak). The gradient is equivalent to  $E/R$ , where  $E$  is the activation energy and  $R$  is the gas constant. Heating rates of 5°, 10°, 20°, and 40°C/min were used to determine the maximum temperature of the exothermic peaks that were positioned at ~500°, 600°, and 700°C.

#### (4) Dilatometry

Crystallization is accompanied by a change in the specimen dimensions. The temperature of maximum activity is determined from the peak in the derivative. Samples that were 12 mm in length and ~1–2 mm thick were prepared. They were heated at a rate of 5°C/min to a maximum temperature of 900°C and then furnace cooled. Other specimens were heated in air to 520°, 630°, and 720°C before air cooling and further analyzed via XRD to identify the phase changes. Thermal events at temperatures >900°C, which is the upper limit for the phase transformations of interest, are not discussed in this paper. Atmospheres of air, helium that was saturated with water vapor, and dry helium were chosen to study the effect of humidity on crystallization. Helium, rather than argon, was chosen because the high thermal conductivity (a factor of six greater than that at 600°C) enables efficient heat transfer to the specimen.<sup>14</sup> A cold trap with liquid nitrogen was used to remove any moisture and produce a dry helium gas. When a high water-vapor pressure was required, water was slowly added to the part of the quartz tube housing that extended from the furnace.

#### (5) Fourier Transform Infrared Spectroscopy

The amorphous powder was mixed with dried potassium bromide (KBr) powder at a concentration of 1 wt% and compressed to produce a transparent tablet. Hydroxyapatite powder and the amorphous phase (after heat treatment at 900°C for 1 h in air and argon) were also examined. An infrared (IR) spectrum with a resolution of 4 cm<sup>-1</sup> and a range of 500–4000 cm<sup>-1</sup> revealed all the major peaks. The carbonate peak that was situated at 2000–2500 cm<sup>-1</sup> results from the background carbon dioxide (CO<sub>2</sub>) within the atmosphere. The librational mode of the hydroxide was detected at 630 cm<sup>-1</sup>; the phosphates exhibited two peaks at slightly less than 610 cm<sup>-1</sup> and three peaks near 1000 cm<sup>-1</sup>.

#### (6) Optical Microscopy

Amorphous coatings were heat treated at 500°, 600°, 650°, and 900°C for 1 h. They were then mounted in epoxy resin and polished according to the procedure that was described by Lugscheider *et al.*<sup>15</sup> A 0.05 µm Al<sub>2</sub>O<sub>3</sub> polishing paste was used on a felt polishing cloth as the final polishing step. This procedure ensured preferential removal of the amorphous phase to reveal

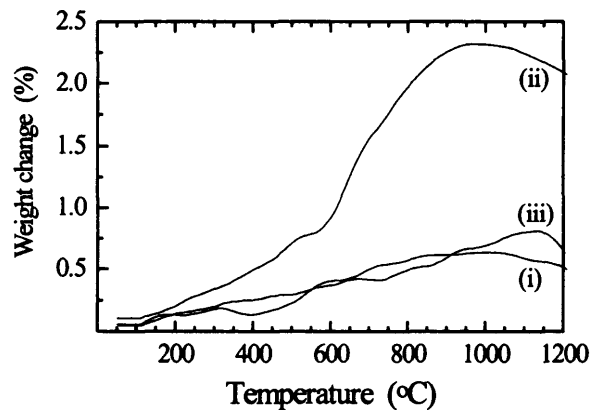
crystalline areas in the coating. Coatings were analyzed using the Nomarski interference method for better depth of field.

### III. Results and Discussion

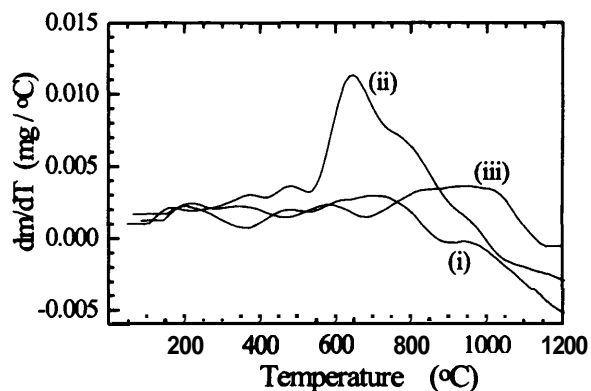
#### (1) Characterization of Starting Powder

The heating of hydroxyapatite commonly causes a decrease in weight. Adsorbed water is removed from the surface at temperatures <200°C and from pores at temperatures up to 500°C, and then structural water is removed at temperatures >900°C.<sup>16–19</sup> If the HPO<sub>4</sub><sup>2-</sup> specie substitutes for the PO<sub>4</sub><sup>3-</sup> specie in the lattice, then heating results in the formation of Ca<sub>2</sub>P<sub>2</sub>O<sub>7</sub>, which is also accompanied by a weight loss.<sup>20</sup> Additional heating then causes a transformation to tricalcium phosphate. Carbonate that occupies either the hydroxide site or a phosphate site can also be relieved by heating at a temperature of ~700°C.<sup>21,22</sup> A weight loss corresponding to the above-mentioned phenomena is not observed. Instead, the opposite trend is reported in the original powder (Fig. 2). The structural water that is lost in the densification stage at temperatures >900°C, prior to the thermal analysis, is replaced when heated in air. This replacement continues until ~1000°C and can be observed from the librational mode of the hydroxyl band that is situated at 630 cm<sup>-1</sup> in the FTIR spectrum (Fig. 3). A greater absorption corresponds to a higher hydroxyl concentration.

The endothermic effect at low temperatures can possibly be attributed to the removal of surface water, which adsorbs to the



(a)



(b)

Fig. 2. (a) TGA showing the weight gain of crystalline hydroxyapatite powder in static air (denoted as "(i)"), the amorphous phase in static air (denoted as "(ii)"), and the amorphous phase in helium at a rate of 15 cm<sup>3</sup>/min (denoted as "(iii)"); (b) the derivative of the weight gain for the same materials as in Fig. 2(a).

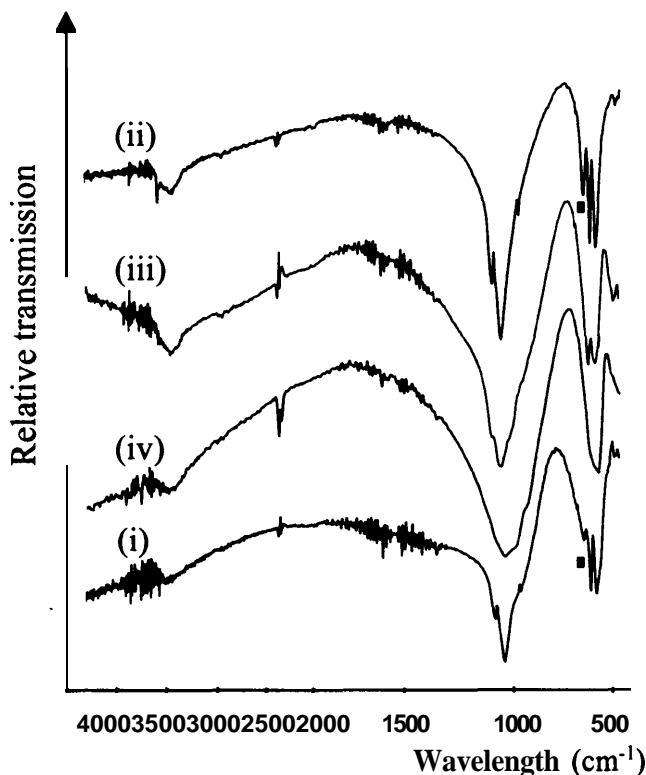


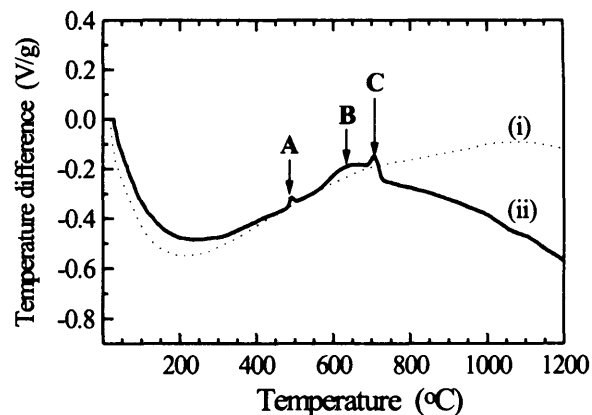
Fig. 3. FTIR spectroscopy of the crystalline hydroxyapatite powder (spectrum "(i)"), the amorphous coating after heat treatment in static air at 900°C (spectrum "(ii)"), the amorphous coating after heat treatment in argon at 900°C (spectrum "(iii)"), and the amorphous phase (spectrum "(iv)"). The librational mode of hydroxide is indicated with a square block at 630  $\text{cm}^{-1}$ .

surface of apatites.<sup>23–26</sup> The DTA trace (Fig. 4(a)) indicates that the adsorbed water is removed at a temperature of 200°C. Shimabayashi and Nakagaki<sup>27</sup> calculated the energy for this desorption to be 5.3 kJ/mol. At higher temperatures, an exothermic tendency prevails until  $\sim 1000^\circ\text{C}$ ; this is partially attributed to the difference in heat capacity between the hydroxyapatite ( $0.7 \text{ J}\cdot(\text{g}\cdot\text{K})^{-1}$  at  $100^\circ\text{C}$ )<sup>28</sup> compared to  $\alpha\text{-Al}_2\text{O}_3$  ( $1.46 \text{ J}\cdot(\text{g}\cdot\text{K})^{-1}$  at  $100^\circ\text{C}$ ).<sup>29</sup> The powder then requires heat for the release of structural water, which indicates an endothermic effect. The thermal behavior of hydroxyapatite at higher temperatures is very composition dependent and can be found elsewhere.<sup>30–32</sup>

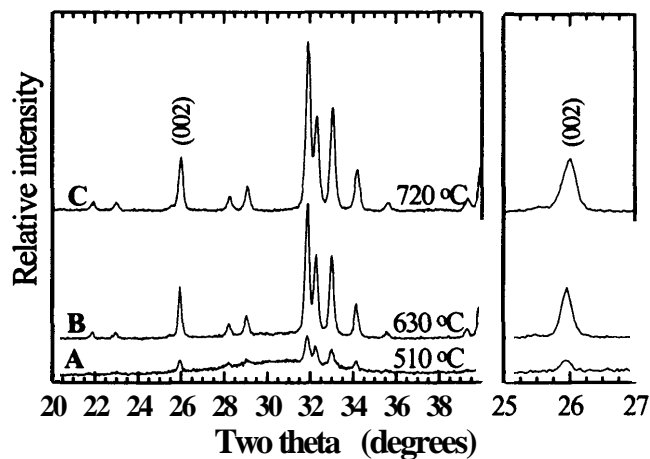
## (2) Hydroxylation of the Amorphous Phase on Heating

TGA of the amorphous phase in air shows a weight gain that, otherwise, is not observed when heat treatment occurs in an inert gas such as helium (Fig. 2). This weight gain results from the uptake of hydroxyl ions into the lattice of hydroxyapatite during crystallization. Supporting evidence is shown in the FTIR spectra in Fig. 3. When the amorphous phase is heat treated in argon, there is no evidence of a hydroxyl presence; however, heat treatment in air results in the appearance of the librational peak that is situated at  $630 \text{ cm}^{-1}$ .

Weight gain occurs up to a temperature of  $900^\circ\text{C}$  with a maximum rate at a temperature of  $\sim 630^\circ\text{C}$ ; this can be used to determine the extent of dehydroxylation within the plasma-spraying process. The total weight gain can be related to the theoretical hydroxide content (3.4 wt%) within hydroxyapatite. Oxyapatite is produced when all the hydroxyl radicals are replaced with half as many oxygen ions. The columns within the hydroxyapatite structure then consist of a row of oxygen ions, each followed by a vacancy. Results from TGA show a weight increase of  $\sim 2.3 \text{ wt}\%$ , which corresponds to a 67% occupation of available hydroxyl ion sites when heating is performed. Because at least 50% of the sites must be occupied for charge



(a)



(b)

Fig. 4. (a) DTA of the crystalline hydroxyapatite powder in static air (curve "(i)") and the amorphous phase in static air (curve "(ii)") ("A" indicates crystallization of hydroxyapatite, "B" indicates the diffusion of hydroxyl ions, and "C" indicates the crystallization of oxyapatite); (b) XRD patterns of amorphous samples heated in the dilatometer to different temperatures (the inset for the range of  $25^\circ$ – $27^\circ$  indicates an increase in the peak width at half height at  $720^\circ\text{C}$ , compared to  $630^\circ\text{C}$ ).

balance (i.e., the case for oxyapatite), heavier species such as carbonates could be included in the columns of the hydroxyapatite structure. The combined results of TGA and FTIR spectroscopy suggest that the amorphous phase was significantly dehydroxylated.

An interesting feature that has been identified in the FTIR spectra is the unusually broad peaks, in addition to the absence of the librational peak at  $630 \text{ cm}^{-1}$ . Peak broadness is attributed, in part, to the stressed phosphate tetrahedra within the coating (as confirmed with Rietveld analysis<sup>33</sup>) and also to the disordered structure that is typical in amorphous materials.

## (3) Crystallization of Hydroxyapatite

DTA of the amorphous phase indicates several phenomena. Well-defined exothermic peaks at  $500^\circ$  and  $700^\circ\text{C}$  and a broad exothermic peak at  $650^\circ\text{C}$  all lie on a slow exothermic rise (Fig. 4). The slow exothermic response could be attributed to structural relaxation, which is common in amorphous materials that have been cooled at a fast rate.<sup>34</sup> During the reheating of

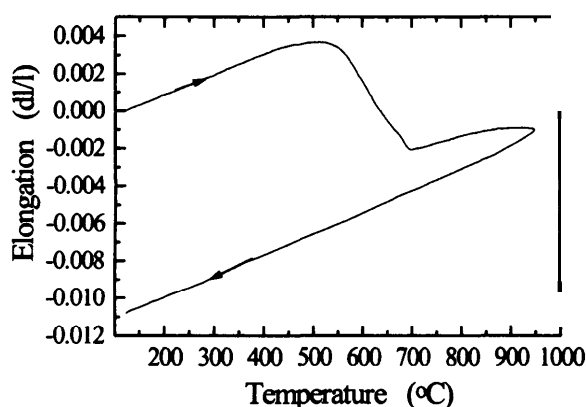
a highly quenched glass, the glass structure adjusts itself to its lowest energy level and, hence, reduces the heat content; this is manifested as a small but recognizable exothermic output, with an accompanying decrease in sample length.<sup>35,36</sup> However, the linear expansion up to 450°C indicates no contraction (Fig. 5), because the sample that was used for dilatometry was possibly relaxed when it was exposed to the elevated temperatures in the coating process. The slowly increasing exotherm also has a contribution from the different heat capacities of the Al<sub>2</sub>O<sub>3</sub> reference and the amorphous phase.

The glass transition, which is accompanied by an endothermic response and an increase in volume, is not observed for the amorphous phase. The transition typically occurs at ~50%–70% of the melting temperature ( $T_m$ )<sup>37</sup> and would correspond to a temperature of ~900°C for the lower limit. Furthermore, a change in the specific heat capacity, occurring during the glass transition, would alter the slope of the DTA curve (Fig. 4). The exothermic peak signifies crystallization before the glass transition is attained, which is a common phenomenon for glasses that are produced by rapid quenching.<sup>37</sup>

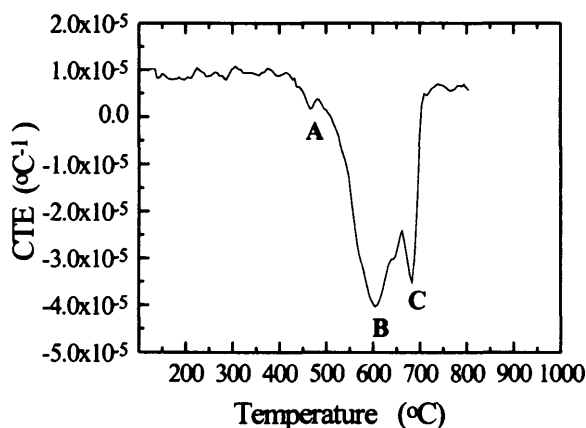
XRD studies were conducted on specimens heated slightly past the temperature of the exothermic peaks detected in the DTA. All three exothermic phenomena are a part of the crystallization process. When heated to 510°C, the XRD pattern shows a crystalline phase that corresponds to an apatitic structure (marked "A" in Fig. 4(b)). The composition of the amorphous phase has a stoichiometric quantity of calcium and phosphorus (i.e., Ca:P ratio of 1.67, as determined experimentally) and allows hydroxyapatite to crystallize.

To differentiate between the crystallization phenomena, dilatometry was conducted in dry helium and water vapor (wet helium) to isolate the effects of the hydroxyl ions in the crystallization process. When dilatometry was conducted in an atmosphere that was saturated with water vapor, crystallization occurred at lower temperatures (Fig. 6(a)). The coefficient of thermal expansion (CTE) indicates that the peak of the activity occurred at ~500°C (Fig. 6(b)), which corresponds to the exothermic peak in DTA (marked "A" in Fig. 4(a)). This peak represents the crystallization of hydroxyl-rich amorphous regions. The exothermic peak that is positioned at ~600°C, which corresponds to peak "B" in Figs. 4(a) and 5(b), signifies the diffusion of hydroxyl ions into hydroxyl-depleted regions, as subsequent crystallization occurs. The crystallization product of hydroxyapatite is confirmed by XRD (Fig. 4(b)).

In the absence of moisture, crystallization occurs at significantly higher temperatures (Fig. 6). The CTE peak at 720°C (Fig. 6(b)) indicates the crystallization of hydroxyl-deficient areas to form oxyapatite. Investigation by XRD is also possible, because the unit cell of oxyapatite is slightly larger in the c-axis, which produces a shift of the (002) peak to lower angles. The slight broadening of the (002) peak that is observed after heat treatment at 720°C, compared to 630°C, occurs from the superposition of the oxyapatite peak onto the hydroxyapatite peak (Fig. 4(b)).

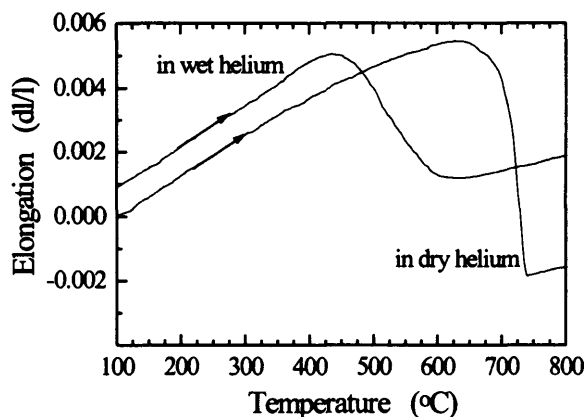


(a)

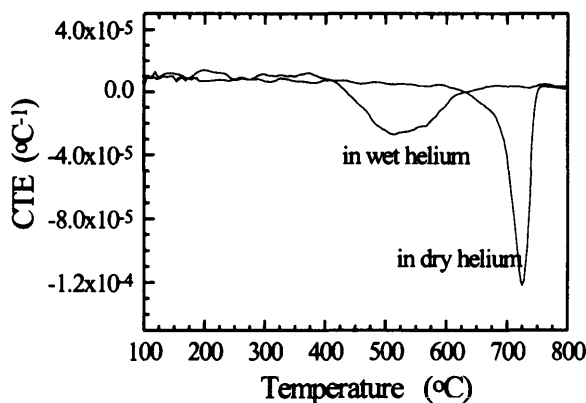


(b)

Fig. 5. (a) Dilatometry curve of the amorphous phase heated in air at 1°C/min; the peaks of activity are shown in Fig. 5(b) as a change in CTE (on heating) and are positioned at 460°, 600°, 640°, and 690°C.



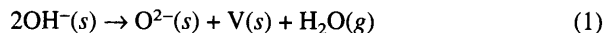
(a)



(b)

Fig. 6. Dilatometry of amorphous hydroxyapatite in wet helium and dry helium showing (a) the change in sample length (elongation) and (b) the CTE, relative to temperature. In Fig. 6(a), an offset in elongation has been introduced for the sample tested in wet helium for ease of observation.

An XRD analysis of the dilatometry samples that have been heated in helium and a high water-vapor pressure illustrate the peak positions for the oxyapatite and hydroxyapatite more clearly (Fig. 7). The high-angle region is chosen where peak separation is greater. Oxyapatite remains stable under dry conditions and will readily transform to hydroxyapatite in the presence of moisture,<sup>38</sup> according to reaction (1), where V represents a vacancy:



The availability of the hydroxyl ions dictates the temperature of the conversion. The two extreme cases that are shown above illustrate the crystallization to hydroxyapatite or oxyapatite. If the heat treatment occurs at a low partial water-vapor pressure, then the initial crystallization product will be a combination of hydroxyapatite and oxyapatite. When heated to temperatures  $>700^\circ\text{C}$ , an uptake of hydroxyl ions, as shown in the results of TGA (Fig. 2), produces an oxy-hydroxyapatite. An oxy-hydroxyapatite represents a unit cell where the concentration of hydroxide ions is different in each column. One column may have two hydroxyl ions, whereas another column may be occupied by an oxygen ion and vacancy. Such a solid solution can be produced in sintered hydroxyapatite ceramics<sup>28</sup> where the time of heat treatment is sufficient to remove the isolated areas of oxyapatite and hydroxyapatite.

The type of apatite that is formed will be determined not only by the availability of the hydroxyl ions but also by the kinetics of the reaction. Crystallization involves reorientation of the phosphate tetrahedra from a distorted configuration and inclusion of an anion for charge balance. The former will partially occur at lower temperatures during structural relaxation. In a hydroxylated amorphous phase, the hydroxide ions provide more charge carriers per unit weight and, therefore, the movement of the anions for crystallization will occur more readily. The activation energy of this process has been calculated as  $274 \pm 2 \text{ kJ/mol}$  (Fig. 8). Crystallization at a temperature of  $-600^\circ\text{C}$  results from the diffusion of hydroxyl species and has an activation energy of  $230 \pm 15 \text{ kJ/mol}$ . The similarity of the reported activation energy with the dehydroxylation of crystalline hydroxyapatite that is associated with an enthalpy change of  $251 \text{ kJ/mol}$ <sup>39</sup> infers that the diffusion of hydroxyl ions could be occurring concurrently in both the amorphous and crystalline phases. The net effect of this diffusion produces crystal growth. The kinetics of the process will be aided if (i) the atmosphere is saturated with water, (ii) energy is released from the stressed phosphate tetrahedra, or (iii) work is performed on the system by hydrostatic pressure. If the amorphous

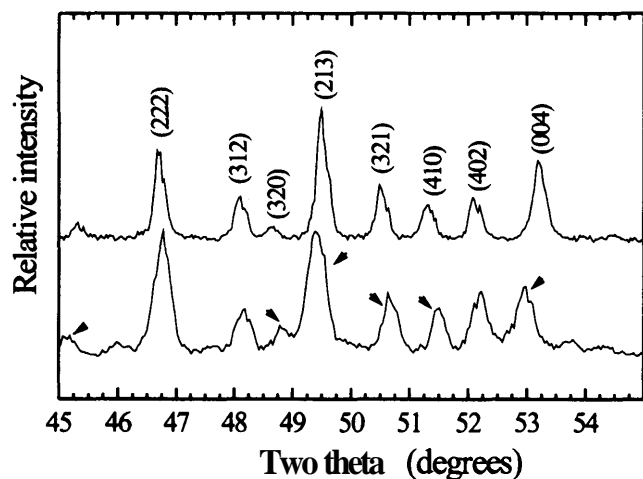


Fig. 7. XRD patterns of the amorphous phase after dilatometry in a dry-helium atmosphere (lower spectra) and helium saturated with water (upper curve). Arrows indicate peak shifts that correspond to oxyapatite.

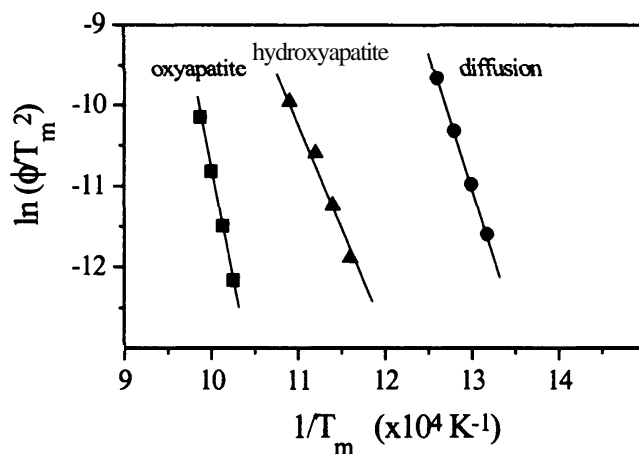


Fig. 8. Activation-energy determination for (A) the crystallization of hydroxyapatite, (■) the crystallization of oxyapatite, and (●) the diffusion of hydroxyl ions, using the method of Kissinger.<sup>11</sup>

phase remains dehydroxylated, as represented by the outside of a flattened particle in a plasma-sprayed coating, then oxyapatite will form. The high activation energy of  $440 \pm 10 \text{ kJ/mol}$  signifies the difficulty of oxygen-anion migration through the amorphous phase to crystallize oxyapatite.

A time-temperature-transformation diagram, if produced for the crystallization, would have components of oxyapatite and hydroxyapatite, the latter being crystallized more easily and extending to lower temperatures. Heat treatment of an amorphous phase in air at  $400^\circ\text{C}$  for 48 h has shown no transformation at this low temperature. Thus, the first crystallization is expected to occur at  $\sim 500^\circ\text{C}$ , as shown by the DTA curve (Fig. 4(a)). The crystallization of hydroxyapatite, which is composition dependent, can be promoted by the presence of water vapor, hydrostatic pressure, or a combination of these, such as that in an autoclave. Crystallization of hydroxyapatite coatings on dental implants during autoclaving is one option to increase the amount of crystalline phase.<sup>40</sup> Because the residual stress varies from coating to coating, the crystallization temperature for any two coatings will be different.

#### (4) Crack Formation

The contraction of the amorphous calcium phosphate is due to the combined effect of crystallization and hydroxylation. The crystallization can be detected at a temperature of  $500^\circ\text{C}$  as growth in preferential directions, which creates interconnected crystalline-phase regions (Fig. 9(a)); in this figure, amorphous regions are indicated with the letter "a" and crystalline areas are identified with the letter "c"). Cracking becomes evident, noticeable as distinct black lines within the crystallized regions after heat treatment at  $600^\circ\text{C}$ , where the hydroxylated areas crystallize (Fig. 9(b)). At a temperature of  $\sim 700^\circ\text{C}$ , the only phase remaining to crystallize is oxyapatite. These dehydroxylated amorphous regions could be the small isolated pockets that are a darker shade of gray, in comparison to the crystallized hydroxyapatite, in Fig. 9(c). Additional heating causes crystallization to oxyapatite. Because hydroxyapatite is 3% denser than oxyapatite,<sup>41</sup> hydroxylation will produce an additional 0.6% contraction. When hydroxylation occurs, these regions become a part of the hydroxyapatite matrix, as viewed by the microstructure at a temperature of  $900^\circ\text{C}$  (Fig. 9(d)).

An interfacial layer appears between the coating and the substrate at higher temperatures (Fig. 9(d)). Several studies have addressed the interfacial reactions between titanium and hydroxyapatite. The phosphate component of hydroxyapatite will not diffuse, because of the size of the groups. Calcium oxide (CaO) will then leave the lattice and react with the titanium oxide ( $\text{TiO}_2$ ) on the substrate. Ji *et al.*<sup>42</sup> used electron microscopy and found  $\text{CaTi}_2\text{O}_5$  between a plasma-sprayed

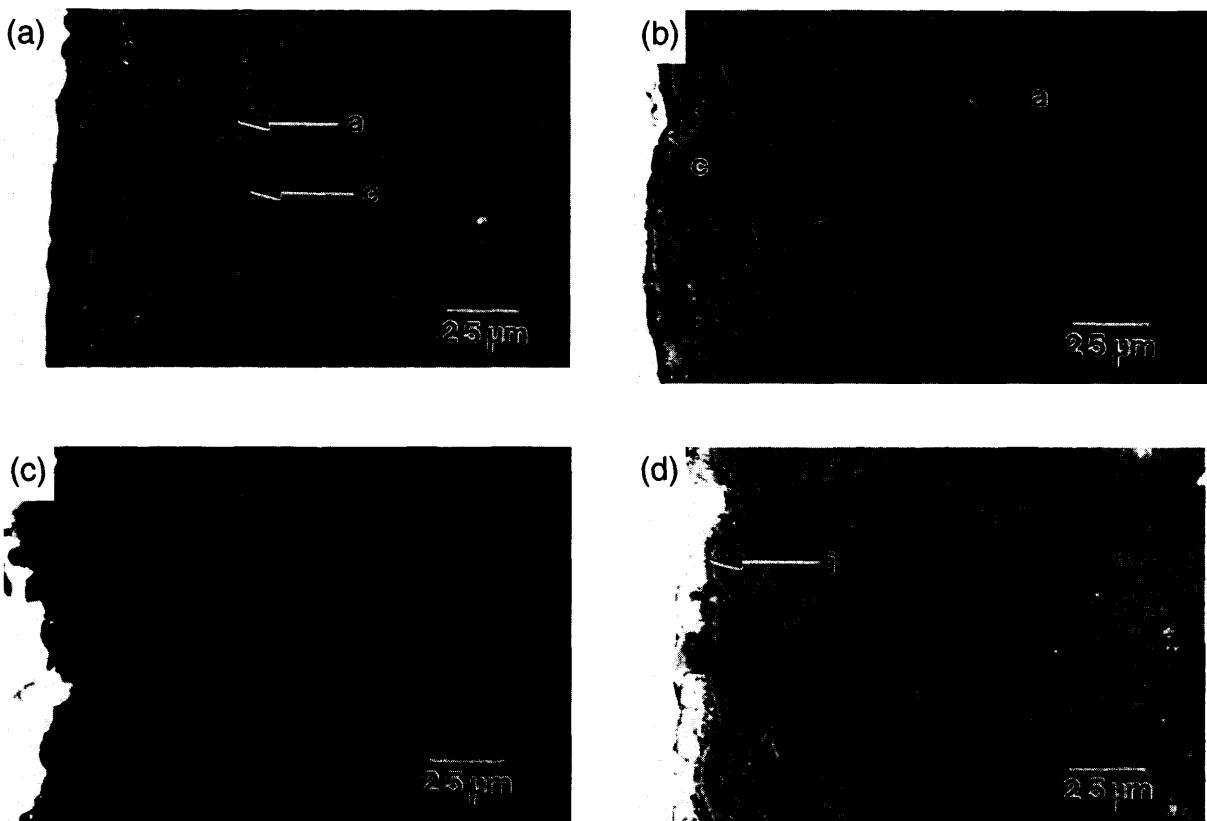


Fig. 9. Optical micrographs of the amorphous phase heat treated at (a) 500°, (b) 600°, (c) 650°, and (d) 900°C, showing presence of amorphous phase (denoted by "a"), crystallized regions (denoted by "c"), an interfacial layer (denoted by "i"), and cracks; the titanium substrate is the white area to the left of each micrograph.

coating and the substrate. However, this material is not an equilibrium phase and will transform to a perovskite,  $\text{CaTiO}_3$ , as anticipated from the phase diagram<sup>43</sup> and also shown by experiment<sup>44,45</sup>

Contraction of the amorphous calcium phosphate manifests itself as a significant reduction in linear expansion when heating occurs (Figs. 5 and 6). The apparent contraction when crystallization occurs corresponds to  $-1\%$  in a direction parallel to the lamellae within the coating. The contraction is approximately proportional to the amount of amorphous phase, with a deviation at high amorphous contents (Table I). One possible reason for this deviation is the variation in size, morphology, distribution, and connectivity of the crystalline regions in coatings of different crystallinity. When a connected crystalline network is established, additional crystallization must break the rigid support before shrinkage can continue. The true shrinkage is composed of the apparent contraction (measured by dilatometry) and crack formation, as observed in the optical micrographs (Fig. 9). Summation of the crack widths produces the total shrinkage within the specimen that was not registered by dilatometry. If the amorphous material was heat treated to 900°C and assuming that no cracks were formed, an additional 5% contraction would occur. Thus, most of the contraction is converted to the formation of cracks. Sintering contributions to the densification are negligible<sup>46-48</sup> but are more important where sintering will produce a large change

in the crystal size. The anisotropy of thermally sprayed coatings would cause a different degree of contraction if this were to be measured perpendicular to the substrate, as indicated in prior studies on zirconia ( $\text{ZrO}_2$ ) coatings.<sup>49</sup>

The appearance of cracking signifies that heat treatment of the amorphous phase is not a favorable option when large changes in crystallinity must be made. Cracking will result in poor adhesion properties to the substrate; thus, delamination of the coatings after crystallization has been occasionally observed. Failure could also occur after implantation, where the cracks could provide a pathway for physiological liquids to cause the separation of the coating from the substrate coating.

A small increase in crystallinity can be produced in this fashion, with limited control over crystallization sites within the coating. The amorphous phase that is located adjacent to the substrate will be more hydroxyl-rich, because of the higher cooling that is experienced by the first layer of the coating.<sup>50</sup> Thus, heat treatment at a temperature of  $-500^\circ\text{C}$  will crystallize the majority of the amorphous phase in this location. Higher temperatures would be required to crystallize the remainder of the amorphous phase.

#### IV. Conclusion

The amorphous phase is predominantly a dehydroxylated calcium phosphate. Heat treatment of the amorphous phase produces crystallization that is dependent on the hydroxyl content of the coating and the humidity. Crystallization initially occurs in the hydroxyl-rich areas of the amorphous phase. The activation energy for this process is 274 kJ/mol. This process is followed by the diffusion of hydroxyl ions through the amorphous phase to produce a crystalline hydroxyapatite (230 kJ/mol). Hydroxyl-depleted areas then crystallize to oxyapatite (440 kJ/mol). When heated, the amorphous phase contracts, because of crystallization and hydroxylation, which produces

Table I. Change in Specimen Length of Different Crystallinity

Amorphous content (wt%)	Change in length (%)
45	0.57
98	0.82

cracks in the coating; this leads to the degradation of material properties such as adhesion strength of the coating and enhanced dissolution through a crack network. Therefore, the presence of large increases in crystalline content of coatings on dental and orthopedic prostheses is not recommended.

## References

- <sup>1</sup>J. F. Kay, "Calcium Phosphate Coatings for Dental Implants—Current Status and Future Potential," *Dent. Clin. North Am.*, **36** [1] 1–18 (1992).
- <sup>2</sup>J. Huracek and P. Spirig, "The Effect of Hydroxyapatite Coating on the Fixation of Hip Prosthesis. A Comparison of Clinical and Radiographic Results of Hip Replacement in a Matched Pair Study," *Arch. Orthop. Traum. Surg.*, **113** [2] 72–77 (1994).
- <sup>3</sup>S. Hurson, "Differentiation of HA Coatings," *J. Dent. Symp.*, **1**, 65–66 (1993).
- <sup>4</sup>R. G. Courtney-Harris, M. V. Kayser, and S. Downes, "Comparison of the Early Production of Extracellular Matrix on Dense Hydroxyapatite and Hydroxyapatite-Coated Titanium in Cell and Organ Culture," *Biomaterials*, **16** [6] 489–95 (1995).
- <sup>5</sup>R. Z. LeGeros, "Biodegradation and Bioresorption of Calcium Phosphate Ceramics," *Clin. Mater.*, **14**, 65–88 (1993).
- <sup>6</sup>F. Brossa, A. Cigada, R. Chiesa, L. Paracchini, and C. Consonni, "Post-deposition Treatment Effects on Hydroxyapatite Vacuum Plasma Spray Coatings," *Biomaterials*, **5** [12] 855–57 (1994).
- <sup>7</sup>M. J. Filiaggi, R. M. Pilliar, and N. A. Coombs, "Post-plasma-spraying Heat Treatment of the HA Coating/Ti-6Al-4V Implant System," *J. Biomed. Mater. Res.*, **27**, 191–98 (1993).
- <sup>8</sup>T. S. Chen and W. R. Lacey, "Crystallization of Ion Beam Deposited Calcium Phosphate Coatings," *J. Mater. Res.*, **9** [5] 1284–90 (1994).
- <sup>9</sup>Z. Zyman, J. Weng, X. Liu, X. Li, and X. Zhang, "Phase and Structural Changes in Hydroxyapatite Coatings under Heat Treatment," *Biomaterials*, **15** [2] 151–55 (1994).
- <sup>10</sup>B. C. Wang, E. Chang, T. M. Lee, and C. Y. Yang, "Changes in Phases and Crystallinity of Plasma-Sprayed Hydroxyapatite Coatings under Heat Treatment: A Quantitative Study," *J. Biomed. Mater. Res.*, **29**, 1483–92 (1995).
- <sup>11</sup>H. E. Kissinger, "Reaction Kinetics in Differential Thermal Analysis," *Anal. Chem.*, **29**, 1702–706 (1956).
- <sup>12</sup>S. Risbud, "Estimation from DTA Traces of the Activation Energy of Crystallization of Glassy CdGeAs<sub>2</sub>," *J. Am. Ceram. Soc.*, **56** [8] 440–41 (1973).
- <sup>13</sup>W. F. Hammett and R. E. Loehman, "Crystallization Kinetics of a Complex Lithium Silicate Glass-Ceramic," *J. Am. Ceram. Soc.*, **70** [8] 577–82 (1987).
- <sup>14</sup>W. Weinlandt, *Thermal Analysis*; p. 22. Wiley, New York, 1986.
- <sup>15</sup>E. Lugscheider, D. Koch, Th. Weber, and M. Knepper, "Metallographische Praeparation von Plasmagespritzten Hydroxyapatitschichten," *Sonderbd. Prakt. Metallogr.*, **22**, 227–36 (1991).
- <sup>16</sup>H. Furedi-Milhofer, V. Hlady, F. S. Baker, R. A. Beebe, N. W. Wikhom, and J. S. Kittelberger, "Temperature-Programmed Dehydration of Hydroxyapatite," *J. Colloid Interface Sci.*, **70** [1] 1–9 (1979).
- <sup>17</sup>H. C. W. Skinner, J. S. Kittelberger, and R. A. Beebe, "Thermal Instability in Synthetic Hydroxyapatites," *J. Phys. Chem.*, **79** [19] 2016–19 (1975).
- <sup>18</sup>H. Owada, K. Yamashita, and T. Kanazawa, "High-Temperature Stability of Hydroxyl Ions in Yttrium-Substituted Oxyhydroxyapatites," *J. Mater. Sci. Lett.*, **9**, 26–28 (1990).
- <sup>19</sup>M. A. Larmas, H. Hayrynen, and L. H. J. Lajunen, "Thermogravimetric Studies on Sound and Carious Human Enamel and Dentin as Well as Hydroxyapatite," *Scand. J. Dent. Res.*, **101**, 185–91 (1993).
- <sup>20</sup>E. E. Berry, "The Structure and Composition of Some Calcium-Deficient Apatites," *J. Inorg. Nucl. Chem.*, **29**, 317–27 (1967).
- <sup>21</sup>J. Arends, J. Christoffersen, M. R. Christoffersen, H. Eckert, B. O. Fowler, J. C. Heughebaert, G. H. Nancollas, J. P. Yesinowski, and S. J. Zawacki, "A Calcium Hydroxyapatite Precipitated from an Aqueous Solution—An International Multimethod Analysis," *J. Cryst. Growth*, **84**, 515–32 (1987).
- <sup>22</sup>M. Jemal and I. Khattech, "Simultaneous Thermogravimetry and Gas Chromatography during Decomposition of Carbonate Apatites," *Thermochim. Acta*, **152**, 65–76 (1989).
- <sup>23</sup>P. A. Timmins and J. C. Wall, "Bone Water," *Calcif. Tissue Res.*, **23**, 1–5 (1977).
- <sup>24</sup>R. Z. LeGeros, G. Bonel, and R. Legros, "Types of 'H<sub>2</sub>O' in Human Enamel and in Precipitated Apatites," *Calcif. Tissue Res.*, **26**, 111–18 (1978).
- <sup>25</sup>A. S. Posner, "The Structure of Bone Apatite Surfaces," *J. Biomed. Mater. Res.*, **19** [3] 241–50 (1985).
- <sup>26</sup>D. N. Misra, "Water on Apatites," *Calcif. Tissue Int.*, **38**, 333–38 (1986).
- <sup>27</sup>S. Shimabayashi and M. Nakagaki, "Dehydration and Change in the Structure of Hydroxyapatite by Heating" (in Jpn.), *Nippon Kagaku Kaishi*, **3**, 3 263 1 (1978).
- <sup>28</sup>T. Kijima and M. Tsutsumi, "Preparation and Thermal Properties of Dense Polycrystalline Oxyhydroxyapatite," *J. Am. Ceram. Soc.*, **62** [9–10] 455–60 (1979).
- <sup>29</sup>W. H. Gitzen, *Alumina as a Ceramic Material*. American Ceramic Society, Columbus, OH, 1970.
- <sup>30</sup>B. Locardi, U. E. Pazzaglia, C. Gabbi, and B. Profilo, "Thermal Behaviour of Hydroxyapatite Intended for Medical Applications," *Biomaterials*, **14** [6] 437–41 (1993).
- <sup>31</sup>J. Zhou, X. Zhang, J. Chen, S. Zeng, and K. de Groot, "High Temperature Characteristics of Synthetic Hydroxyapatite," *J. Mater. Sci.: Mater. Med.*, **4**, 83–85 (1993).
- <sup>32</sup>Y. Fang, D. K. Agrawal, and D. M. Roy, "Thermal Stability of Synthetic Hydroxyapatite"; pp. 269–82 in *Hydroxyapatite and Related Materials*. Edited by P. W. Brown and B. Constanz. CRC Press, Boca Raton, FL, 1994.
- <sup>33</sup>J. C. Knowles, K. A. Gross, C. C. Bemdt, and W. Bonfield, "Structural Changes Induced during Thermally Spraying of Hydroxyapatite. A Comparison of Three Different Spraying Methods"; pp. 311–16 in *Bioceramics 8*. Edited by J. Wilson, L. L. Hench, and D. Greenspan. Butterworth-Heinemann, London, U.K., 1995.
- <sup>34</sup>L. D. Pye, H. J. Stevens, and W. C. LaCourse, *Introduction to Glass Science*. Plenum Press, New York, 1972.
- <sup>35</sup>E. Etchessahar, M. Harmelin, and J. Debuigne, "Structural Relaxation, Glass Transition and Crystallization of Cu-Zr Amorphous Ribbons Studied by Dilatometry and Differential Scanning Calorimetry," *Thermochim. Acta*, **142**, 29–47 (1989).
- <sup>36</sup>H. Friedrichs and H. Neuhauser, "Study of Structural Relaxation of Metallic Glasses by Stress-Free Dilatometry," *J. Phys.: Condens. Matter*, **1**, 8305–18 (1989).
- <sup>37</sup>H. S. Chen and K. A. Jackson, "Metallic Glasses"; pp. 215–60 in *Ultra-rapid Quenching of Liquid Alloys*. Edited by H. Herman. Academic Press, New York, 1981.
- <sup>38</sup>G. Montel, G. Bonel, J. C. Trombe, J. C. Heughebaert, and C. Rey, "Progress dans le Domaine de la Chimie des Composés Phosphore Solides a Structure d'Apatite," *Pure Appl. Chem.*, **52**, 973 (1980).
- <sup>39</sup>A. M. J. H. Seuter, "Existence Region of Calcium Hydroxylapatite and the Equilibrium with Coexisting Phases at Elevated Temperatures"; pp. 806–12 in *Reactivity of Solids*. Edited by J. S. Anderson, M. W. Roberts, and F. S. Stone. Chapman and Hall, London, U.K., 1972.
- <sup>40</sup>S. Hurson; private communication, 1995.
- <sup>41</sup>J. C. Trombe and G. Montel, "Some Features of the Incorporation of Oxygen in Different Oxidation States in the Apatitic Lattice," *J. Inorg. Nucl. Chem.*, **40**, 15–21 (1978).
- <sup>42</sup>H. Ji, C. B. Ponton, and P. M. Marquis, "Microstructural Characterization of Hydroxyapatite Coating on Titanium," *J. Mater. Sci.: Mater. Med.*, **3**, 283–87 (1992).
- <sup>43</sup>R. S. Roth, J. R. Dennis, and H. F. McMurdle, *Phase Diagrams for Ceramists, Vol. VI*; pp. 110–11. American Ceramic Society, Columbus, OH, 1987.
- <sup>44</sup>J. L. Lacout, J. Assarane, and J. C. Trombe, "Fixation of Titanium by Phosphate Minerals," *C. R. Acad. Sci.*, **298** [5] 173–75 (1984).
- <sup>45</sup>C. Chai and B. Ben-Nissan, "Interfacial Reactions between Titanium and Hydroxyapatite," *J. Aust. Ceram. Soc.*, **29** [1/2] 71–80 (1993).
- <sup>46</sup>G. De With, J. A. van Dijk, N. Hattus, and K. Prijs, "Preparation, Microstructure and Mechanical Properties of Dense Polycrystalline Hydroxyapatite," *J. Mater. Sci.*, **16** [6] 1592–98 (1981).
- <sup>47</sup>P. E. Wang and T. K. Chaki, "Sintering Behaviour and Mechanical Properties of Hydroxyapatite and Dicalcium Phosphate," *J. Mater. Sci.: Mater. Med.*, **4** [2] 150–58 (1993).
- <sup>48</sup>P. Van Landuyt, F. Li, J. P. Keustermans, J. M. Streydio, F. Delannay, and E. Munting, "The Influence of High Sintering Temperatures on the Mechanical Properties of Hydroxylapatite," *J. Mater. Sci.: Mater. Med.*, **6**, 8–13 (1995).
- <sup>49</sup>D. Wang and C. C. Berndt, "Anisotropic Thermal Expansion Behaviour of Thermally Sprayed Coatings"; pp. 295–304 in *Proceedings of the 2nd Plasma Technik Symposium, Vol. 2*. Edited by S. Blum-Sansmeier, H. Eschnauer, P. Huber, and A. R. Nicoll. Hafliger Druck AG, Luzern, Switzerland, 1991.
- <sup>50</sup>K. A. Gross, "The Amorphous Phase in Hydroxyapatite Coatings"; Ph.D. Dissertation. State University of New York at Stony Brook, Stony Brook, NY, 1995. □